# A higher-order tangent linear parabolic-equation solution of three-dimensional sound propagation

**Ying-Tsong Lin**
*Applied Ocean Physics and Engineering Department, Woods Hole Oceanographic Institution, Woods Hole, Massachusetts 02543*
*ytlin@whoi.edu*

**Abstract:** A higher-order square-root operator splitting algorithm is employed to derive a tangent linear solution for the three-dimensional parabolic wave equation due to small variations of the sound speed in the medium. The solution shown in this paper unifies other solutions obtained from less accurate approximations. Examples of three-dimensional acoustic ducts are presented to demonstrate the accuracy of the solution. Future work on the applications of associated adjoint models for acoustic inversions is proposed and discussed.


**PACS numbers:** 43.20.Bi, 43.30.Dr [WS]
**Date Received:** May 20, 2013 **Date Accepted:** July 1, 2013

## 1. Introduction

Sound propagation can be affected by the temporal and spatial variability of acoustic properties in the medium, and this paper presents a tangent linear solution for the sound field variability due to small variations of the sound speed. Although not detailed in this paper, this tangent linear solution can also lead to adjoint models for acoustic inversions and sensitivity analysis. Earlier development of this modeling technique was for meteorology and ocean dynamics, and it was later extended for acoustics, e.g., by Hursky *et al.* (2004) and Hermand *et al.* (2006). The solution presented in this paper is based on the parabolic-equation (PE) method, and the contribution of this work is to extend the previous formulations of Hursky *et al.* (2004) and Smith (2006) for three-dimensional (3D) sound propagation and for better accuracy by employing a higher-order square-root operator splitting algorithm (Lin and Duda, 2012).

A brief introduction to the previous work is provided here. Consider the following one-way parabolic wave equation,

$$\frac{\partial}{\partial x}u(x,y,z) = ik_{\text{ref}}\left\{-1+\sqrt{k_{\text{ref}}^{-2}\nabla_{\perp}^{2}+n^{2}(x,y,z)}\right\}u(x,y,z) = ik_{\text{ref}}\,\mathcal{L}\,u(x,y,z). \quad (1)$$

Here, the Cartesian coordinate system is selected to achieve a uniform resolution, and the parabolic wave equation can also be expressed in the same form using cylindrical coordinates. In Eq. (1), $u$ is the demodulated sound pressure with the baseline phase removed according to the reference wavenumber $k_{\text{ref}}$, i.e., $u(x,y,z) = p(x,y,z) \times \exp(-ik_{\text{ref}}x)$, and $\nabla_{\perp}^{2} = (\partial^2/\partial y^2 + \partial^2/\partial z^2)$ is the two-dimensional (2D) Laplacian. Besides, the exact PE operator consisting of the square-root Helmholtz operator is

$$\mathcal{L} = -1+\sqrt{k_{\text{ref}}^{-2}\nabla_{\perp}^{2}+n^{2}(x,y,z)}, \quad (2)$$

where $n$ is the index of refraction with respect to $k_{\text{ref}}$. For simplicity of the presentation, the medium density variable is neglected in Eq. (1) without loss of generality. If needed, the density variable can be either incorporated into the 2D Laplacian $\nabla_{\perp}^{2}$ (Collins, 1993) or transferred into an effective index of refraction (Bergmann, 1946). Now consider

$$n^2(x,y,z) = \gamma_0(x,y,z) + \varepsilon\gamma_1(x,y,z), \tag{3}$$

where $\gamma_0$ is the square of the index of refraction of the background state, and $\gamma_1$ is a perturbation scaled by an arbitrary small parameter $\varepsilon$. Hursky *et al.* (2004) showed that the standard narrow-angle PE operator (Tappert, 1977) has the following linear approximation with respect to $\gamma_1$:

$$\mathcal{L}_1 = \frac{1}{2}(k_{\text{ref}}^{-2}\nabla_\perp^2 + \gamma_0 - 1) + \frac{1}{2}\varepsilon\gamma_1. \tag{4}$$

Later, Smith (2006) showed another approximation for the wide-angle PE operator (Feit and Fleck, 1978):

$$\mathcal{L}_2 = -2 + \sqrt{1 + k_{\text{ref}}^{-2}\nabla_\perp^2} + n_0 + \varepsilon n_1, \tag{5}$$

where the medium perturbation is directly expressed in terms of the index of refraction, $n = n_0 + \varepsilon n_1$. In this paper, a new approximation that generalizes $\mathcal{L}_1$ and $\mathcal{L}_2$ will be derived using the following higher-order square-root operator splitting scheme (Lin and Duda, 2012):

$$\sqrt{1+\mathcal{A}+\mathcal{B}} \cong -1 + \sqrt{1+\mathcal{A}} + \sqrt{1+\mathcal{B}} - \frac{1}{2}[(-1+\sqrt{1+\mathcal{A}})(-1+\sqrt{1+\mathcal{B}}) + (-1+\sqrt{1+\mathcal{B}})(-1+\sqrt{1+\mathcal{A}})], \tag{6}$$

where the symbols $\mathcal{A}$ and $\mathcal{B}$ denote general operators.

## 2. Theory

Derivation of the new approximated PE operator that generalizes $\mathcal{L}_1$ and $\mathcal{L}_2$ is straightforward by substituting $n^2(x,\ y,\ z) = \gamma_0(x,\ y,\ z) + \varepsilon\gamma_1(x,\ y,\ z)$ in the exact PE operator $\mathcal{L}$, Eq. (2), and then employing the higher-order square-root operator splitting scheme, Eq. (6), with $\mathcal{A} = -1 + \gamma_0 + k_{\text{ref}}^{-2}\nabla_\perp^2$ and $\mathcal{B} = \varepsilon\gamma_1$. This yields

$$\mathcal{L}_3 = \mathcal{L}_0 + \frac{1}{2}[(1-\mathcal{L}_0)(-1+\sqrt{1+\varepsilon\gamma_1}) + (-1+\sqrt{1+\varepsilon\gamma_1})(1-\mathcal{L}_0)], \tag{7}$$

where $\mathcal{L}_0 = -1 + \sqrt{\gamma_0 + k_{\text{ref}}^{-2}\nabla_\perp^2}$ is the background PE operator. The rest of the section is focused on solving a parabolic wave equation composed of $\mathcal{L}_3$, $\partial u / \partial x = ik_{\text{ref}}\mathcal{L}_3 u$, to obtain the higher-order tangent linear PE solution.

We first use the same perturbation parameter $\varepsilon$ to decompose the demodulated sound pressure, i.e., $u(x,y,z) = \sum_{m=0}^{\infty}\varepsilon^m u_m(x,y,z)$. Then, substituting the perturbation expansion of $u$ in the parabolic wave equation of $\mathcal{L}_3$ and collecting terms of the same order in $\varepsilon$ yields the next set of equations for each expansion component $u_m$:

$$\mathbb{O}(1): \quad \frac{\partial u_0}{\partial x} = ik_{\text{ref}}\mathcal{L}_0 u_0, \tag{8a}$$

$$\mathbb{O}(\varepsilon^m): \quad \frac{\partial u_m}{\partial x} \cong ik_{\text{ref}}\mathcal{L}_0 u_m + \frac{ik_{\text{ref}}}{4}[(1-\mathcal{L}_0)\gamma_1 + \gamma_1(1-\mathcal{L}_0)]u_{m-1} \quad \text{for} \quad m \geq 1, \tag{8b}$$

where the order of $\gamma_1$ is kept linear by approximating $\sqrt{1+\varepsilon\gamma_1}$ in $\mathcal{L}_3$ as $1 + \varepsilon\gamma_1/2$.

Equation (8a) is a standard parabolic partial differential equation, and its solution is $u_0(x+\Delta x) = e^{ik_{\text{ref}}\Delta x\mathcal{L}_0}u_0(x)$ with an assumption of negligible or nonexistent $x$-dependency

in $\mathcal{L}_0$ from $x$ to $x+\Delta x$. To solve Eq. (8b), we need to first calculate the higher derivatives of $u_m$, i.e.,

$$\frac{\partial^\ell u_m}{\partial x^\ell} \cong (ik_{\text{ref}}\mathcal{L}_0)^\ell u_m + \frac{(ik_{\text{ref}})^\ell}{4}\sum_{j=0}^{\ell-1}\mathcal{L}_0^j[(1-\mathcal{L}_0)\gamma_1 + \gamma_1(1-\mathcal{L}_0)]\mathcal{L}_0^{\ell-j-1}u_{m-1}$$
$$\text{for} \quad m \geq 1 \quad \text{and} \quad \ell \geq 2. \tag{9}$$

Then, using the Taylor series expansion $u_m(x+\Delta x) = \sum_{\ell=0}^{\infty}(\ell!)^{-1}(\Delta x)^\ell \partial^\ell u_m(x)/\partial x^\ell$, we can determine the solution of Eq. (8b) with an additional assumption of negligible or nonexistent $x$-dependency in $\gamma_1$ from $x$ to $x+\Delta x$. Finally, substituting $u_0(x+\Delta x)$ and $u_m(x+\Delta x)$ in the perturbation expansion leads to the higher-order tangent linear PE solution of $\mathcal{L}_3$:

$$\mathcal{L}_3: \quad u(x+\Delta x) \cong e^{ik_{\text{ref}}\Delta x\mathcal{L}_0}u(x) + \frac{1}{4}\sum_{\ell=1}^{\infty}\frac{(ik_{\text{ref}}\Delta x)^\ell}{\ell!}\sum_{j=0}^{\ell-1}\mathcal{L}_0^j[(1-\mathcal{L}_0)\varepsilon\gamma_1 + \varepsilon\gamma_1(1-\mathcal{L}_0)]\mathcal{L}_0^{\ell-j-1}u(x). \tag{10}$$

Because the refractive index perturbations are small in the applications of interest, we can further assume commutativity between $\mathcal{L}_0$ and $\gamma_1$. So, Eq. (10) can be rewritten as

$$\mathcal{L}_3: \quad u(x+\Delta x) \cong e^{ik_{\text{ref}}\Delta x\mathcal{L}_0}\left[1 + \frac{ik_{\text{ref}}}{2}\Delta x(1-\mathcal{L}_0)\varepsilon\gamma_1\right]u(x), \tag{11}$$

where the higher-order terms in $\Delta x$ in Eq. (10) are retained to form the exponential operator. One can see that, before marching to $x+\Delta x$ with the background PE propagator $e^{ik_{\text{ref}}\Delta x\mathcal{L}_0}$, the tangent linear correction $ik_{\text{ref}}\Delta x(1-\mathcal{L}_0)\varepsilon\gamma_1 u(x)/2$ for the medium perturbation $\varepsilon\gamma_1$ is applied to $u(x)$, and the higher-order component of the correction is $-ik_{\text{ref}}\Delta x\mathcal{L}_0\varepsilon\gamma_1 u(x)/2$.

Following similar procedures one can also find the narrow-angle and wide-angle tangent linear solutions resulted from $\mathcal{L}_1$ and $\mathcal{L}_2$, respectively:

$$\mathcal{L}_1: \quad u(x+\Delta x) \cong e^{ik_{\text{ref}}\Delta x[k_{\text{ref}}^{-2}\nabla_\perp^2 + n_0^2 - 1]/2}\left(1 + \frac{ik_{\text{ref}}}{2}\Delta x\varepsilon\gamma_1\right)u(x) \tag{12}$$

and

$$\mathcal{L}_2: \quad u(x+\Delta x) \cong e^{ik_{\text{ref}}\Delta x[-2+\sqrt{1+k_{\text{ref}}^{-2}\nabla_\perp^2}+n_0]}(1 + ik_{\text{ref}}\Delta x\varepsilon n_1)u(x). \tag{13}$$

Note that Eq. (11) will reduce to Eq. (12) when the higher-order correction is neglected, and when the background PE propagator $e^{ik_{\text{ref}}\Delta x\mathcal{L}_0}$ is approximated by the standard narrow-angle PE method, $\mathcal{L}_0 \cong (k_{\text{ref}}^{-2}\nabla_\perp^2 + \gamma_0 - 1)/2$. Similarly, Eq. (11) will reduce to Eq. (13) if the background PE propagator is approximated by the wide-angle PE method, $\mathcal{L}_0 \cong -2 + \sqrt{1 + k_{\text{ref}}^{-2}\nabla_\perp^2} + n_0$. In Sec. 3, we will directly compare these three solutions and demonstrate that the higher-order tangent linear solution resulted from $\mathcal{L}_3$ is most accurate.

Although it will not be presented as an example, the tangent linear solution introduced in this paper can lead to an adjoint model. One approach is briefed as follows. The derivation starts with keeping only the first two terms in the perturbation expansion of $u$, i.e., $u \cong u_0 + \varepsilon u_1$. By substituting this linear perturbation expansion in Eq. (11), we can obtain a marching equation to determine $u_1(x+\Delta x)$ from the value of $u_0$, $u_1$, and $\gamma_1$ at $x$,

$$u_1(x+\Delta x) \cong e^{ik_{\text{ref}}\Delta x\mathcal{L}_0}\left\{u_1(x)+\left[\frac{ik_{\text{ref}}}{2}\Delta x(1-\mathcal{L}_0)\gamma_1\right]u_0(x)\right\}. \quad (14)$$

Equation (14) can in fact be rewritten in a compact form $u_1(x+\Delta x) \cong \mathcal{F}\,u_1(x) + \mathcal{Q}\,\gamma_1\,u_0(x)$, and it is readily suited for the procedure proposed by Hursky *et al.* (2004) to construct the associated adjoint model. The details are omitted here, and interested readers are referred to Hursky *et al.* (2004).

## 3. Numerical examples

A higher-order split-step Fourier scheme introduced by Lin and Duda (2012) is employed here to implement the background PE propagator $e^{ik_{\text{ref}}\Delta x\mathcal{L}_0}$ and the higher-order correction $-ik_{\text{ref}}\Delta x\mathcal{L}_0\varepsilon\gamma_1 u(x)/2$. An example of underwater sound propagation over an idealized slope is presented to demonstrate the solution accuracy. The geometry of this idealized problem is shown in Fig. 1(a), and the model parameters are as follows. The slope is 5°, and the water column is homogeneous with sound speed 1500 m/s, density 1 g/cm$^3$, and no medium absorption. The bottom is also homogeneous with sound speed 1700 m/s, density 1 g/cm$^3$, and medium absorption 0.5 dB/wavelength. A 75 Hz point source is located 2 km away from the apex at a depth of 100 m. This idealized slope example is in fact identical to the wedge problem studied by Lin and Duda (2012), where a reference solution obtained from a method of images (Deane and Buckingham, 1993) was used to benchmark the higher-order split-step Fourier PE solution. Here, the image solution is used to check the higher-order tangent linear PE solution [Eq. (11)]. Note that when implementing the higher-order split-step Fourier scheme, the water-bottom interface has to be smoothed. The hyperbolic tangent smoothing procedure suggested by Tappert (1977) is employed here, and the smoothing width is set to be 1.25 m, which is one-sixteenth of the acoustic wavelength in the water at 75 Hz and will not cause significant errors to the PE solution. Also, the numerical convergency of the higher-order split-step Fourier scheme is ensured with the cross-range grid size $\Delta y = 1.5$ m, the depth grid size $\Delta z = 1$ m, and the marching step $\Delta x = 1.25$ m.

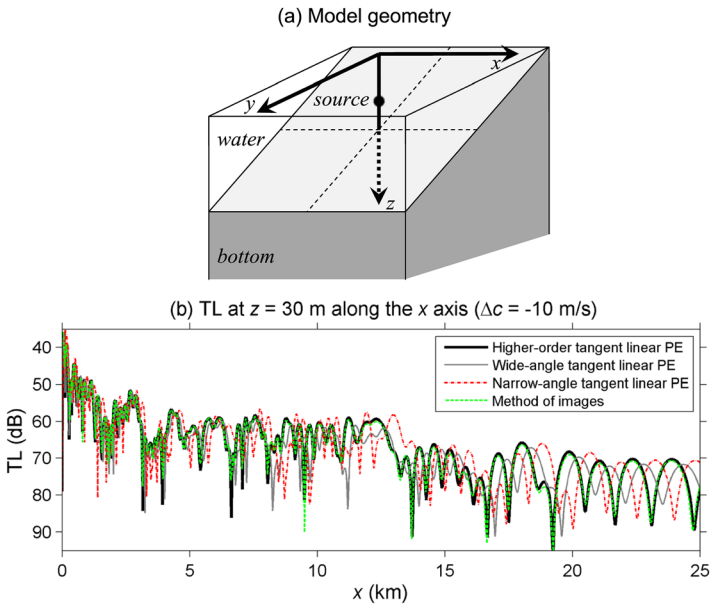


Fig. 1. (Color online) An example of 75 Hz sound propagation in an idealized slope environment. (a) Geometry of the slope model. (b) Comparison of TL solutions at $z = 30$ m along the $x$ axis. Among three different tangent linear PE solutions, the higher-order one has the best agreement with the reference solution obtained from the method of images of Deane and Buckingham (1993).

In the first test, the water sound speed of the background state is set to be 1510 m/s, so it requires the perturbation $\Delta c = -10$ m/s to reach the 1500 m/s sound speed set forth in the slope model parameters. The higher-order tangent linear PE solution of the transmission loss (TL) at $z = 30$ m along the $x$ axis is shown in Fig. 1(b), and the method of images of Deane and Buckingham (1993) is implemented to obtain a reference solution for comparison. In addition to the higher-order solution [Eq. (11)], the narrow-angle and wide-angle tangent linear solutions resulted from $\mathcal{L}_1$ and $\mathcal{L}_2$ [Eqs. (12) and (13)] are also computed. As seen in Fig. 1(b), the higher-order tangent linear solution has the best agreement with the image solution, and the other two tangent linear solutions have significant pattern phase errors in a distance greater than 5 km.

To examine the accuracy of the higher-order tangent linear PE solution corresponding to different sound speed perturbations, the water sound speed of the background state in the idealized slope model is changed from 1470 to 1530 m/s, i.e., $\Delta c$ varies from 30 to $-30$ m/s. Let the higher-order solution with the background sound speed equal to 1500 m/s ($\Delta c = 0$) be the reference, the root-mean-square (rms) error of the TL solution at $z = 30$ m along the $x$ axis is computed and plotted in Fig. 2 as a function of $\Delta c$ (the curve with circles). Small rms errors are achieved for $|\Delta c| < 20$ m/s. A similar computation is also made by neglecting the higher-order correction $-ik_{\mathrm{ref}}\Delta x\mathcal{L}_0\varepsilon\gamma_1 u(x)/2$ to demonstrate its significance. The resultant rms errors are plotted in Fig. 2 as a curve with triangles, and one can clearly see that without applying the higher-order correction the error of the tangent linear solution becomes large.

Another example of the horizontal ducting of sound by a sound speed front over a slope is presented. The sound speed front is caused by a nonlinear internal wave of depression across the slope as shown in Fig. 3(a). There are two layers in the water column, and the upper layer is 20-m thick with sound speed 1520 m/s, as opposed to 1480 m/s in the lower water layer. The rest of the model parameters are described below. The slope is 3°, and the bottom properties follow the idealized slope example. The shape of the internal wave is a hyperbolic secant squared function with amplitude 50 m and width 150 m, and the wave is located at 2.5 km away from the apex. A 75 Hz point source is placed between the apex and the internal wave (500 m to the wave), and the source depth is 50 m.

The higher-order split-step Fourier scheme is also utilized in this internal wave example, with the same computational configuration as the previous example. Figure 3(b) shows the background TL solution on the $x$-$y$ plane at the source depth (50 m) in the absence of the internal wave, and one can see both the cut-off of the sound in the $x$ direction and the interference pattern caused by the horizontal refraction of acoustic modes off the slope. Because the thermocline in the water column is depressed by the internal wave, a 3D acoustic duct is formed. A similar ducting condition is studied analytically by Lin and Lynch (2011), who showed that, due to the joint effect of the off-slope refraction by the sloping bottom and the upslope refraction from the sound speed front, the propagating sound can be trapped between the apex and the front. The higher-order tangent linear solution shown in Fig. 3(c) indeed represents this

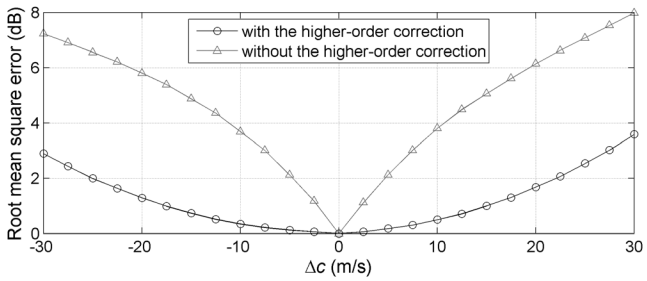


Fig. 2. Error comparison of the higher-order tangent linear PE solution with and without the higher-order correction $-ik_{\mathrm{ref}}\Delta x\mathcal{L}_0\varepsilon\gamma_1 u(x)/2$ in the idealized slope example.

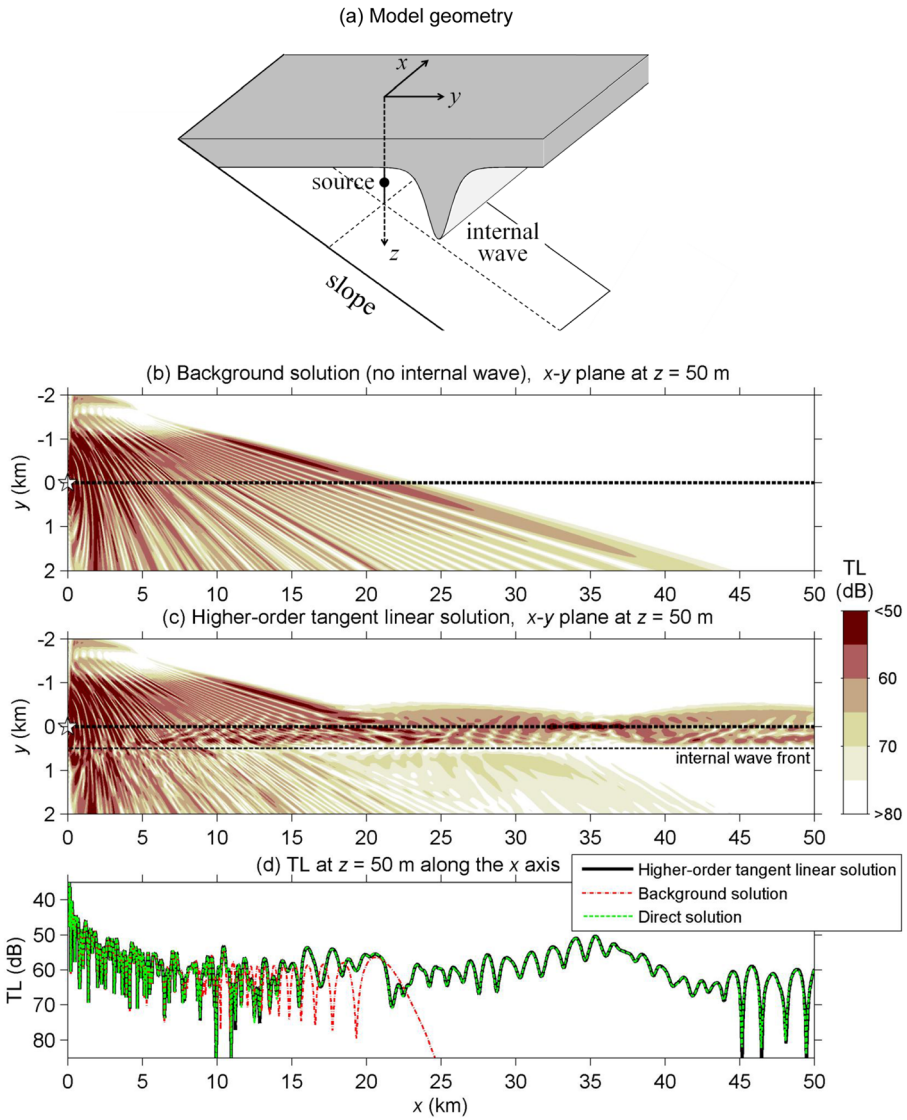


Fig. 3. (Color online) An example of 75 Hz sound propagation in the presence of a nonlinear internal wave over a slope. (a) Geometry of the slope plus internal wave model. (b) The background solution of the TL on the $x$-$y$ plane at $z = 50$ m in the absence of the internal wave. (c) The higher-order tangent linear PE solution of the TL on the $x$-$y$ plane at $z = 50$ m in the presence of the internal wave. (d) Comparison of different TL solutions.

propagation physics. To examine the accuracy of the tangent linear solution, the higher-order split-step Fourier PE solution (Lin and Duda, 2012) is computed directly without using the perturbation formula. As seen in Fig. 3(d), the higher-order tangent linear solution agrees with the direct solution very well. Note that, even though the acoustic ducting condition changes drastically due to the presence of the internal wave, the tangent linear solution can still accurately predict the effects of sound speed variations and track down the sound field variability.

## 4. Summary

A higher-order tangent linear PE solution of 3D sound propagation is derived in this paper, and it unifies other tangent linear PE solutions by employing a higher-order

splitting algorithm for the square-root Helmholtz operator. Numerical examples of 3D sound propagation are presented to show the performance of the solution. The first example considers an idealized slope/wedge problem, and the higher-order tangent linear solution agrees very well with the reference solution obtained from the method of images by Deane and Buckingham (1993). The second example is the horizontal ducting of sound by a sound speed front over a slope. It shows that the tangent linear solution can accurately predict the sound field variability even when the ducting condition changes drastically. Future work on developing associated adjoint models is proposed for acoustic inversions, sensitivity analysis and, as an ultimate goal, acoustic data assimilation in a 3D environment.

## Acknowledgment

This work was sponsored by the Office of Naval Research under Grant No. N00014-13-1-0026.

## References and links

Bergmann, P. G. (**1946**). "The wave equation in a medium with a variable index of refraction," J. Acoust. Soc. Am. **17**, 329–333.

Collins, M. D. (**1993**). "A split-step Padé solution for parabolic equation method," J. Acoust. Soc. Am. **93**, 1736–1742.

Deane, G. B., and Buckingham, M. J. (**1993**). "An analysis of the three-dimensional sound field in a penetrable wedge with a stratified fluid or elastic basement," J. Acoust. Soc. Am. **93**, 1319–1328.

Feit, M. D., and Fleck, J. A., Jr. (**1978**). "Light propagation in graded-index fibers," Appl. Opt. **17**, 3990–3998.

Hermand, J.-P., Meyer, M., Asch, M., and Berrada, M. (**2006**). "Adjoint-based acoustic inversion for the physical characterization of a shallow water environment," J. Acoust. Soc. Am. **119**, 3860–3871.

Hursky, P., Porter, M. B., Cornuelle, B. D., Hodgkiss, W. S., and Kuperman W. A. (**2004**). "Adjoint modeling for acoustic inversion," J. Acoust. Soc. Am. **115**, 607–619.

Lin, Y.-T., and Duda, T. F. (**2012**). "A higher-order split-step Fourier parabolic-equation sound propagation solution scheme," J. Acoust. Soc. Am. **132**, EL61–EL67.

Lin, Y.-T., and Lynch, J. F. (**2011**). "Analytical study of the horizontal ducting of sound by an oceanic front over a slope," J. Acoust. Soc. Am. **131**, EL1–EL7.

Smith, K. B. (**2006**). "Adjoint modeling with a split-step Fourier parabolic equation model (L)," J. Acoust. Soc. Am. **120**, 1190–1191.

Tappert, F. D. (**1977**). "The parabolic equation method," in *Wave Propagation and Underwater Acoustics*, edited by J. B. Keller and J. Papadakis, Lecture Notes in Physics 70 (Springer-Verlag, New York), pp. 224–286.